Effects of shear elasticity on sea bed scattering: Numerical examples.

Anatoliy N. Ivakin
Andreev Acoustics Institute,
Shvernika 4, Moscow 117036, Russia

Darrell R. Jackson
Applied Physics Laboratory, College of Ocean and Fishery Sciences,
1013 N.E. 40th Street, Seattle, Washington 98105-6698

August 16, 1996

Abstract

It is known that marine sediments can support both compressional and shear waves. However, published work on scattering from irregular elastic media has not examined the influence of shear on sea bed scattering in detail. A perturbation model previously developed by the authors for joint roughness-volume scattering is used to study the effects of elasticity for three sea bed types: sedimentary rock, sand with high shear speed, and sand with "normal" shear wave speed. Both bistatic and monostatic cases are considered. For sedimentary rock it is found that shear elasticity tends to increase the importance of volume scattering and decrease the importance of roughness scattering relative to the fluid case. Shear effects are shown to be small for sands.

PACS numbers: 43.30Pc, 43.60Pt, 43.30Gv, 43.30Ma

REPORT DOCUMENTATION PAGE

Form Approved
OMB No. 0704-0188

1. AGENCY USE ONLY (Leave Blank)	2. REPORT DATE	3. REPORT TYPE AND DATES COVERED
	August 16, 1996	Final Report 10/24/94-11/30/96

4. TITLE AND SUBTITLE

Effects of shear elasticity on sea bed scattering: Numerical examples.

5. FUNDING NUMBERS

N00014-95-1-0157

6. AUTHOR(S)

Anatoliy N. Ivakin and Darrell R. Jackson

7. PERFORMING ORGANIZATION NAME(S) AND ADDRESS(ES)

Applied Physics Laboratory
University of Washington
1013 NE 40th Street
Seattle, WA 98105-6698

8. PERFORMING ORGANIZATION REPORT NUMBER

9. SPONSORING/MONITORING AGENCY NAME(S) AND ADDRESS(ES)

Office of Naval Reseach, Code 321OA
800 North Quincy Street
Arlington, VA 22217-5660

10. SPONSORING/MONITORING AGENCY REPORT NUMBER

11. SUPPLIMENTARY NOTES

Submitted to the Journal of the Acoustical Society of America

12a. DISTRIBUTION/AVAILABILITY STATEMENT

Unlimited distribution.

12b. DISTRIBUTION CODE

13. ABSTRACT (Maximum 200 words)

It is known that marine sediments can support both compressional and shear waves. However, published work on scattering from irregular elastic media has not examined the influence of shear on sea bed scattering in detail. A perturbation model previously developed by the authors for joint roughness-volume scattering is used to study the effects of elasticity for three sea bed types: sedimentary rock, sand with high shear speed, and sand with "normal" shear wave speed. Both bistatic and monostatic cases are considered. For sedimentary rock it is found that shear elasticity tends to increase the importance of volume scattering and decrease the importance of roughness scattering relative to the fluid case. Shear effects are shown to be small for sands.

14. SUBJECT TERMS

sea bed scattering
shear elasticity
marine sediments
perturbation model

15. NUMBER OF PAGES

36

16. PRICE CODE

17. SECURITY CLASSIFICATION OF REPORT	18. SECURITY CLASSIFICATION OF THIS PAGE	19. SECURITY CLASSIFICATION OF ABSTRACT	20. LIMITATION OF ABSTRACT
Unclassified	Unclassified	Unclassified	Unlimited

INTRODUCTION

In a previous paper, the Born approximation (first-order perturbation theory) was developed for sound scattering by rough, elastic sea beds [13]. This formalism combines roughness scattering and scattering due to volume inhomogeneities. An example was given showing strong and complicated elasticity effects for roughness and volume scattering for sea bed rock. Essen [6] has used the Born approximation to treat sea bed roughness scattering for types ranging from very soft sediment to basalt. His results indicate that shear effects can be important for sands as well as for consolidated sediments and basalt. Yang and Broschat [21], however, have applied the Born approximation and small-slope approximation to the interface scattering problem and give an example indicating that shear effects should not be important for rough sands. Ivakin [12] reached a similar conclusion with respect to volume scattering from sands.

One purpose of the present article is to provide an evaluation of the importance of shear effects in both volume and roughness scattering from sea bed types ranging from sand to rock along with a comparison of the volume and roughness components of scattering. Another purpose is to study the dependence of volume scattering upon the statistics obeyed by the volume fluctuations, e.g., correlations between volume parameters.

Use of the Born approximation limits the quantitative validity of the results of this article to sea beds having small roughness and relatively low levels of fluctuation in volume parameters. It is expected, however, that our results will have *qualitative* validity more generally. That is, when the Born approximation indicates that shear effects are large, this qualitative statement is likely to be true even when the level of roughness or volume inhomogeneity is sufficient to invalidate the Born approximation.

1 SEA BED STATISTICAL MODEL

It is assumed that a rough interface separates a lossless, homogeneous fluid (representing sea water) from an inhomogeneous elastic sea bed medium. Bulk properties of the sea bed are defined by density, ρ, and compressional and shear wave speeds, c_p and c_t . Subscripts, p and t, here and below denote longitudinal (compressional) and transverse (shear) waves, respectively. In

the water, c_t is taken to be zero.

The sea bed parameters will be divided into two classes: those representing the average, non-fluctuating values of bulk properties such as density and wave speeds, and those describing sea bed random properties. The former are defined by the seabed type and will be assigned values appropriate to sand and rock. The latter are defined by the statistics of the random fluctuation of bulk parameters and interface relief.

1.1 Average Properties

The average sea bed parameters of interest are as follows. The density ratio, $a_\rho = \rho/\rho_f$, is the ratio of the average sediment mass density to that of the overlying water. The compressional wave speed ratio, $a_p = c_p/c_f$, is likewise the ratio of the average sediment compressional wave speed, c_p, and the water compressional wave speed, c_f. This ratio is complex, with imaginary part determining absorption loss. The shear speed ratio, $a_t = c_t/c_f$, is the ratio of the average complex sediment shear speed, c_t, and the compressional wave speed in the water. The "loss parameters" [14, 18] can be expressed in terms of the real and imaginary parts of the compressional and shear speed ratios

$$\delta_\alpha = -\frac{Im[a_\alpha]}{Re[a_\alpha]} \tag{1}$$

where the subscript $\alpha = p, t$ denotes the wave type in the seabed.

1.2 Model for Roughness

The roughness two-dimensional (2-D) spectrum is taken to be of the form

$$\Phi_2^{(r)}(\mathbf{K}) = \frac{B^{(r)}}{(K^2 + K_0^2)^{\gamma_r/2}} \tag{2}$$

where $\mathbf{K} = (K_1, K_2)$, $K = \sqrt{K_1^2 + K_2^2}$. Equation 2 assumes that roughness statistics are stationary and isotropic, with a spectrum that obeys a power law for $K^2 \gg K_0^2$. The parameter K_0 is an inverse correlation scale for roughness in the transverse directions. The roughness spectrum strength, $B^{(r)}$, and the power exponent, γ_r, can be estimated, as shown below, from available one-dimensional (1-D) data.

The integral over all $\mathbf{K}$ (including negative spatial frequencies) of the spectrum yields the mean-square roughness,

$$h^2 = \int \Phi_2^{(r)}(\mathbf{K}) d^2K \tag{3}$$

This gives the following expression for the dimensionless spectral strength:

$$B^{(r)} = h^2 K_0^{\gamma_r - 2}(\gamma_r/2 - 1)/\pi \quad . \tag{4}$$

This requires $\gamma_r > 2$, but this is shown below to be usually valid.

Most of available data on roughness properties are in the form of one-dimensional spectra, $\Phi_1^{(r)}(K_1)$. Usually they can be well approximated by the power law

$$\Phi_1^{(r)}(K_1) = \frac{A^{(r)} h_0^{3-\xi_r}}{K_1^{\xi_r}}, \; K_1 \gg K_0. \tag{5}$$

The trivial parameter $h_0 = 1$ m is introduced for convenience to yield a dimensionless roughness spectrum strength, $A^{(r)}$. Typical measured values (see, e.g., [2]) are $A^{(r)} \approx 10^{-6}$ to 10^{-2}, and $\xi_r \approx 1$ to 3.

The relation between 1-D and 2-D spectra is given by the integral

$$\Phi_1^{(r)}(K_1) = \int \Phi_2^{(r)}(\mathbf{K})\, dK_2.$$

Then, using Eq. 2, one obtains

$$\Phi_1^{(r)}(K_1) = \frac{2B^{(r)}}{(K_1^2 + K_0^2)^{(\gamma_r - 1)/2}} \int_0^\infty \frac{dx}{(x^2+1)^{\gamma_r/2}}. \tag{6}$$

Comparing 6 to 5, one obtains the relation between parameters $B^{(r)}$ and $A^{(r)}$, γ_r and ξ_r,

$$\gamma_r = \xi_r + 1, \tag{7}$$

$$B^{(r)} = h_0^{3-\xi_r} F(\xi_r) A^{(r)}, \tag{8}$$

where

$$F(\xi_r) = \frac{\Gamma\left(\frac{1+\xi_r}{2}\right)}{\Gamma(1/2)\Gamma(\xi_r/2)}, \tag{9}$$

with Γ being the gamma function. In particular, one obtains $F(1) = 1/\pi, F(2) = 1/2$, $F(3) = 2/\pi$, $F(4) = 3/4$. This generalizes the result, given in Ref. [14] for the case $K_0 = 0$. Note that $\xi_r \approx 1$ to 3 corresponds to $\gamma_r \approx 2$ to 4.

1.3 Model for Volume Inhomogeneities

A description of the statistics of volume inhomogeneities is given by a matrix of spatial (3-dimensional) cross-spectra. These are Fourier transforms of cross-correlation functions for the relative fluctuations $\epsilon_\rho = \Delta\rho/\rho, \epsilon_p = \Delta c_p/c_p, \epsilon_t = \Delta c_t/c_t$. These relative fluctuations will be collectively designated ϵ_β with $\beta = \rho, p, t$. In this notation, the cross-spectra are taken to be of the form

$$\Phi^{(v)}_{\beta\beta'}(\mathbf{K},q) = \frac{B_{\beta\beta'}}{(q_0^2 + q^2 + K^2a^2)^{\gamma_v/2}}. \tag{10}$$

This equation assumes that inhomogeneity statistics are stationary and isotropic in transverse directions, with a spectrum that obeys a power law if $q^2 + K^2a^2 \gg q_0^2$. The parameter q_0 is an inverse correlation scale for inhomogeneities in the vertical direction. The so-called aspect ratio, a, specifies the anisotropy of the inhomogeneities and is the ratio of horizontal to vertical correlation scales [11, 24, 22, 23]. For $a = 1$, the inhomogeneities are isotropic on the average and have a spherical form (referring to surfaces of constant correlation in spatial lag space). For $a \gg 1$, the inhomogeneities are strongly anisotropic and constant correlation surfaces are thin oblate ellipsoids. Generally, in the case of transverse anisotropy, one more aspect ratio must be introduced corresponding to the third correlation scale [4]. Angular coordinates for orientation of the inhomogeneity ellipsoids in space can also be arbitrarily introduced [22, 23].

The three-dimensional integrals analogous to Eq. 3 are the elements of the covariance matrix for volume fluctuations

$$< \epsilon_\beta \epsilon^*_{\beta'} >= \int \Phi^{(v)}_{\beta\beta'}(\mathbf{K}, q) d^2K\, dq\ . \tag{11}$$

These integrals are infinite if $\gamma_v \leq 3$ but can be made finite for all γ_v if a high frequency cutoff is introduced. Accordingly, it will be assumed that

$$\Phi^{(v)}_{\beta\beta'}(\mathbf{K},q) = 0 \tag{12}$$

for

$$K^2a^2 + q^2 > (q_0/\varepsilon)^2, \ \varepsilon \ll 1. \tag{13}$$

Introduction of the small dimensionless cutoff parameter, ε, provides smooth behavior of the corresponding correlation functions for small spatial lags and also yields finite variance for the inhomogeneity fluctuations for any γ_v. Obviously, this is important as experimental data have finite variance and have finite spatial resolution with respect to both large and small scales. The "small" spatial lags for which the cutoff has effect have scales comparable to, or smaller than the components of the vector $(a, a, 1)\varepsilon/q_0$.

The matrix elements $B_{\beta\beta'}$ can be determined from Equation 11 (see Appendix). Otherwise, available geoacoustic data can be used for the estimation of the spectrum parameters. In the case of strongly correlated or anticorrelated fluctuations one can consider any one of the three fluctuations, say density, as defining the other two. This parameter will be called the "reference" parameter. In this case, put

$$\epsilon_\beta = r_{\beta\rho}\epsilon_\rho, \tag{14}$$

where the corresponding speed fluctuation ratios (with respect to fluctuations of the density) are

$$r_{\beta\rho} = \frac{\rho}{c_\beta}\left(\frac{\partial c_\beta}{\partial \rho}\right), \ \beta = p, t, \tag{15}$$

where $r_{\beta\rho}$ can be taken from compilations of geoacoustic data, for example Hamilton's [7, 9, 10, 8] and others [17, 20]. In this case

$$B_{\beta\beta'} = r_{\beta\rho}\, r_{\beta'\rho}\, B_{\rho\rho}. \tag{16}$$

for all combinations of β and β', with $r_{\rho\rho} = 1$.

The parameters $B_{\rho\rho}$ and γ_v can be also obtained from available data. Most data on fluctuations of bulk properties provide only one-dimensional (vertical) spectra, $\Phi_1^{(v)}(q)$. Usually they can be well approximated by the power law

$$\Phi_1^{(v)}(q) = \frac{A^{(v)} h_0^{1-\xi_v}}{q^{\xi_v}}, \ q \gg q_0. \tag{17}$$

Again, the parameter $h_0 = 1$ m is used to obtain a dimensionless spectrum strength, $A^{(v)}$. Typical measured values (see, e.g., [1, 3, 16, 22, 24]) are $A^{(v)} \approx$

10^{-5} to $10^{-2}, \xi_v \approx 0.5$ to 2. Typical estimates obtained from inversions of geoacoustical data [11, 22, 24] are $a \approx 1$ to 10.

The relation between 1-D and 3-D spectra, generalized in Ref. [24] for anisotropic inhomogeneities with aspect ratio a, is given by the expression

$$\Phi_3^{(v)}(q') = -\frac{a^2}{2\pi q'} \frac{d\Phi_1^{(v)}(q')}{dq'},$$

where

$$q' = \sqrt{q^2 + K^2 a^2}.$$

Then, using Eq. 17, one obtains the relation between parameters $B^{(v)}$ and $A^{(v)}$, γ_v and ξ_v,

$$\gamma_v = \xi_v + 2,$$

$$B^{(v)} = h_0^{1-\xi_v} A^{(v)} a^2 \xi_v / (2\pi).$$

2 NUMERICAL EXAMPLES

To illustrate the effects of shear elasticity, we consider scattering from sea beds of varying composition, ranging from sand to solid rock. Finer-grained silts and clays are not considered, as their low shear speeds [6, 19] result in negligible shear effects. The parameters c_p, c_t, and ρ that characterize these examples were chosen primarily to illustrate certain points rather than to provide extensive coverage of a range of realistic sea bed types. Some of the chosen examples are fairly realistic, others are not. The parameters specified below were used in computing angular dependencies of the scattering strength. With regard to roughness scattering, some of the effects seen in the present example are visible in other published work [5, 21, 6]. The intent here is to compare and contrast elasticity effects as they appear in roughness *and* volume scattering.

2.1 Scattering Strength

In this section, the expressions given in [13] are used for calculation of scattering strength, $10\log\sigma$, where σ is the scattering cross section per unit area of the sea bed and characterizes the frequency- angular distribution of the mean intensity of field fluctuations in the Fraunhofer zone (or far zone, relative to a scattering surface or volume). The scattering cross section is assumed to be the sum of contributions from interface roughness and volume inhomogeneity in the form

$$\sigma = \sigma_r(\mathbf{K}_s, \mathbf{K}_i) + \sigma_v(\mathbf{K}_s, \mathbf{K}_i)$$

where σ_r and σ_v are components due to roughness and volume scattering, respectively, $\mathbf{K}_s$ and $\mathbf{K}_i$ are horizontal (transverse) components of the scattered and incident wave vectors, correspondingly. Vectors $\mathbf{K}_s$ and $\mathbf{K}_i$ are expressed through the essential angular coordinates of the problem

$$\mathbf{K}_{s,i} = (k_f \cos\theta_{s,i} \cos\phi_{s,i},\ k_f \cos\theta_{s,i} \sin\phi_{s,i}) \ . \tag{18}$$

These are: grazing angles, θ_i and θ_s, for the incident and scattered acoustic waves, respectively, and the azimuths, ϕ_s and ϕ_i for the incident and scattered waves (see Figure 1). Frequency enters through the acoustic wave number in the water $k_f = \omega/c_f$. Roughness and volume scattering cross sections, σ_r and σ_v, are expressed in terms of the average parameters of the seabed, a_ρ, a_p, a_t, and its statistical parameters, the two-dimensional spatial spectra of roughness, $\Phi^{(r)}(\mathbf{K})$, and the three-dimensional cross-spectra of different volume fluctuations, $\Phi^{(v)}_{\beta\beta'}(\mathbf{K},q)$, where $\mathbf{K} = \mathbf{K}_s - \mathbf{K}_i$ and q is the vertical component of the spectral argument [13].

2.2 Input parameters

Table 1 lists the average properties of the three sea bed types chosen for illustration of the effects of elasticity on acoustic scattering. These sea bed types include a strongly elastic case (sedimentary rock), a moderately elastic case (sand with unusually high shear speed, "shear" sand), and a weakly elastic case (sand with a more typical, "moderate", shear speed).

Two different sets of random parameters are used for sands and rock. The roughness and volume parameters are specified below.

The roughness spectral parameters were assigned the values used in Ref [13]: $\gamma_r = 4, K_0 = 10^{-2}\mathrm{m}^{-1}$ and $B^{(r)} = (2/\pi) \times A^{(r)}$ with $A^{(r)} = 10^{-5}$, with the factor $(2/\pi)$ resulting from the relation between 2-D and 1-D roughness spectra.

The reference (density) inhomogeneity spectrum was taken to be of the form given in Eq. 10 with $\gamma_v = 3$, $q_0 = 10^{-2}\mathrm{m}^{-1}$, $B^{(v)}_{\rho\rho} = (2\pi)^{-1}a^2 \times A^{(v)}$ and $A^{(v)} = 10^{-5}$. Again, these parameters were used in Ref. [13], except, here, the aspect ratio is not taken to be unity. The parameter $B^{(v)}_{\rho\rho}$ contains a factor $a^2/(2\pi)$ resulting from the relation between 3-D and 1-D spectra. The corresponding one-dimensional (vertical) spectrum is simply $A^{(v)}/K$, which gives a reasonable fit to the available data [24].

In the "correlated" case, the cross spectrum matrix elements were calculated using Eq. 16 with the ratios $r_{\beta\rho}$ estimated from published relations between geoacoustic parameters [10, 17] and listed in Table 2 for the sea bed types chosen for illustration.

In another case to be considered, the elements of the correlation matrix are taken to be of the form

$$B^{(v)}_{\beta\beta'} = \delta_{\beta\beta'} r^2_{\beta\rho} B^{(v)}_{\rho\rho}. \tag{19}$$

Because of the Kroneker delta used in Eq. 19, all the nondiagonal elements of the correlation matrix vanish. In this "uncorrelated" case, the volume component of the scattering cross section, according to [13], will be simply the sum of three components

$$\sigma_v = \sum_\beta \sigma^{(v)}_\beta \tag{20}$$

where $\sigma^{(v)}_\beta$ correspond to contributions of fluctuations of the three different bulk parameters ($\beta = \rho, c_p, c_t$).

Calculations are presented both for the sum and for each of the terms in Eq. 20. The former permits an evaluation of the role of cross correlations between different volume fluctuations, or nondiagonal elements of the correlation matrix, by comparison of the two extremes: the strongly correlated case and the uncorrelated case. The latter permits a comparison of the the role of different fluctuations.

3 DISCUSSION

The first example to be considered uses parameters appropriate to sedimentary rock [6]. As the set of figures used in this and following examples is rather involved, an explanation of the arrangement of the figures will be given before discussing the results. Figure 2 shows the monostatic or backscattering case, giving the dependence of scattering strength on backscattering grazing angle. Figure 3 shows the dependence of bistatic scattering strength upon scattered grazing angle with the incident grazing angle fixed at 45° and the difference between scattered and incident azimuth fixed at 180°. As the scattered grazing angle varies from 0° to 180°, it passes through the backscatter direction (45°) and the forward, or "specular", direction (135°). Figure 4 shows the dependence of bistatic scattering strength upon the difference between scattered and incident azimuthal angles at fixed incidence and scattered grazing angles, both taken to be 45°. All three figures compare the elastic and fluid cases. In the fluid case, the shear wave speed is set to zero and all other parameters are kept the same as in the elastic case. Each of the figures is divided into parts (a) and (b). Part (a) compares three separate cases: roughness scattering, correlated volume scattering and uncorrelated volume scattering. Part (b) compares separate volume scattering mechanisms, fluctuations in density, compressional wave speed, and shear wave speed.

For sedimentary rock, the effects of shear elasticity on both roughness and volume scattering are very strong, as illustrated by Figs. 2-4. Noteworthy effects are:

- Figures 2a and 3a show that roughness scattering strength exhibits dips at grazing angles immediately below the critical angles for shear and compressional waves (39.7° and 64.2°, respectively).

- Shear elasticity decreases roughness scattering strength compared to the fluid case for grazing angles less than the shear critical angle and near the forward direction (Figs. 2a, 3a, and 4a).

- Elasticity greatly enhances scattering strength for volume scattering in the directions where it decreases roughness scattering (Figs. 2-4). The effects for volume scattering are much larger than the effects for roughness scattering.

- For grazing angles below the compressional critical angle, scattering due to density fluctuations has nearly the same angular dependence as scattering due to shear speed fluctuations (Figs. 2b and 3b).

- The effect of cross-correlation for different perturbations can be large, as it is noticeable in Fig. 3a from the difference between correlated and uncorrelated cases in the range 60° - 120°.

The influence of shear elasticity in surficial sands is expected to be rather small as they typically have shear speeds much lower than the water compressional wave speed (see, e.g., [10, 20]). For illustrative purposes, therefore, an example will first be considered in which shear effects are exaggerated. This example is used by Essen [6] and is distinguished by a shear speed of 480 m/s. This case of sand with high shear speed, the "shear" sand case, is illustrated in Figs. 5-7. These figures show the following effects:

- Both roughness and volume backscattering (Fig. 5a) are reduced relative to the fluid case for grazing angles smaller than the compressional critical angle (33.6°). Compared to the sedimentary rock example, this is the same behavior regarding roughness but the opposite regarding volume scattering.

- The relative contributions of volume and roughness scattering (Figs. 5a, 6a, 7a) are very dependent on scattering angle. Roughness scattering is dominant near the specular direction, but volume scattering can be important for incident or scattering angles greater than the compressional critical angle.

- The effect of cross-correlation for different perturbations can be large, as it is noticable from the difference between correlated and uncorrelated cases in Fig. 6a (in the range 80° to 180°) and in Fig. 7a (-100° to 100°). Note that this difference is negligible in the fluid case.

- Volume scattering in backward directions for sands (Figs. 5b, 6b, 7b) is mostly due to density fluctuations, while both compressional and shear wave speed fluctuations are unimportant. But, at the same time, even weak fluctuations of compressional speed (an order of magnitude smaller than density fluctuations) can be important near the forward direction (Fig. 6b). Shear fluctuations also provide significant scattering near the forward direction (Figs. 6b, 7b).

The last example, with scattering strength shown in Figs. 8 and 9, is a sand with shear speed of about 200 m/s, similar to typical measured values [10, 19]. Here again, the relative importance of roughness and volume scattering is dependent upon angle. Density fluctuations are generally more important than compressional speed fluctuations in the backscattering case (Fig. 8) with relatively reduced contribution in forward directions (Fig. 9). These effects have little to do with shear elasticity, however. In fact, the effects of shear elasticity are negligible for both roughness and volume scat-

tering. Scattering by shear speed fluctuations in forward and near specular directions is about 10 dB lower than scattering by density and compressional speed fluctuations (Fig. 9) and absolutely negligible in the backscattering case (the shear component is not seen in Fig. 9 as its level is too low). Thus, even though sand is definitely a shear-supporting medium in a geotechnical sense, it can be treated by a simple fluid acoustic model.

The effects of elasticity on roughness and volume scattering for rock can be summarized by saying that elasticity "softens" the interface, decreasing the acoustic contrast with water with a corresponding decrease in reflection and roughness scattering and a corresponding increase in transmission and volume scattering. This view is substantiated by Fig. 10, which compares the magnitudes of reflection and transmission coefficients for the fluid and elastic cases. In the fluid case, the reflection coefficient is very nearly equal to unity for grazing angles below the compressional critical angle. The inclusion of lossy shear greatly alters this picture, with the energy reflection coefficient dropping to very small values for grazing angles in the vicinity of 35°. This causes the decrease noted in roughness scattering. At the same time, Fig. 10 shows that the transmission coefficient for pressure waves is greatly increased when elastic effects are included. The conversion to shear energy is also efficient, and both effects enhance volume scattering. The opposite effect for scattering in high-shear-speed sand, mentioned above, is explained analogously by Fig. 11.

For the sedimentary rock example, when the incident and scattered grazing angles are less than the compressional critical angle, only incident and scattered vertically polarized shear waves are important. Thus, there is no interference between different scattering channels; only shear-to-shear scattering is important. This causes the similarity observed in the angular dependences of scattering by density and shear speed fluctuations. The scattering levels due to these two mechanisms are different only because different fluctuation levels are assumed (Table 2).

4 CONCLUSIONS

First-order perturbation theory results obtained in [13] have been used to study the effects of shear elasticity on acoustic scattering by sea beds of different types. While the calculations presented here are quantitatively correct

only in a region of small roughness and small volume fluctuations, it is likely that the general conclusions drawn from these examples will be qualitatively valid outside this region.

With respect to scattering by rock, shear elasticity weakens roughness scattering and strengthens volume scattering. Surprisingly, this suggests that volume scattering may sometimes dominate, or at least compete with, roughness scattering, in sharp contrast to the predictions of the fluid model. The other general conclusion resulting from these examples, is that sand can be treated as an acoustic fluid. This reinforces the results presented by Yang and Broschat [21].

ACKNOWLEDGMENTS

We wish to acknowledge the support of the Office of Naval Research.

Appendix: Volume Cross Spectrum Matrix

The matrix elements, $B_{\beta\beta'}$, can be determined from Equation 11 which gives

$$B_{\beta\beta'} = \sigma_\beta \sigma_{\beta'} R_{\beta\beta'} a^2 q_0^{\gamma_v - 3} (\gamma_v/2 - 1)/[\pi Q(\gamma_v, \varepsilon)]$$

where

$$\sigma_\beta = \sqrt{< |\epsilon_\beta|^2 >}$$

are the standard deviations of the three different fluctuation types, and

$$R_{\beta\beta'} = \frac{< \epsilon_\beta \epsilon^*_{\beta'} >}{\sigma_\beta \sigma_{\beta'}}$$

are their cross-correlation coefficients. In the case of strongly correlated or anticorrelated fluctuations one can put $R_{\beta\beta'} = \pm 1$ respectively, and in the "uncorrelated" case, $R_{\beta\beta'} = \delta_{\beta\beta'}$. The parameter $Q(\gamma_v, \varepsilon)$ is a dimensionless normalizing factor

$$Q(\gamma, \varepsilon) = 2 \int_0^{1/\varepsilon} \frac{1}{(1 + x^2)^{\gamma/2 - 1}} \, dx.$$

For $\gamma_v = 3$, one obtains

$$Q \approx 2 \ln(1/\varepsilon) ,$$

while, for $\gamma_v < 3$,

$$Q \approx 2\,\varepsilon^{-(3-\gamma_v)}/(3-\gamma_v) ,$$

and, for $\gamma_v > 3$,

$$Q \approx Q(\gamma_v, 0) = \Gamma(1/2)\Gamma(\gamma_v/2 - 3/2)/\Gamma(\gamma_v/2 - 1) , \qquad (21)$$

For $\gamma_v = 4$, in particular, $Q = \pi$. Expression 21 is exact if $\varepsilon = 0$.

References

[1] T.Akal, "Acoustical characteristics of the sea floor: Experimental techniques and some examples from the Mediterranean sea", in: *Physics of Sound in Marine Sediments,* ed. by L. Hampton, Plenum Press, New York, 1974, pp. 447-480.

[2] K. B. Briggs, "Microtopographical roughness of shallow-water continental shelves," *IEEE J. Oceanic Engr.,* **14**, 360-367 (Oct. 1989).

[3] K. B. Briggs, "High-frequency acoustic scattering from sediment interface roughness and volume inhomogeneities," Naval Research Laboratory, NRL/FR/7431–94-9617, Dec. 1994.

[4] A. V. Bunchuk and A. N. Ivakin, "Azimuthal anisotropy of sound backscattering from the ocean bottom in shallow water," in: V Seminar on Acoustic and Statistical Models of the Ocean, 1985, pp.47-51 (in Russian).

[5] D. K. Dacol and D. H. Berman, "Sound scattering from a randomly rough fluid-solid interface," *J. Acoust. Soc. Am.*, **84**, 292–302 (1988).

[6] H. H. Essen, "Scattering from a rough sedimental seafloor containing shear and layering," *J. Acoust. Soc. Am.,* **95**, 1299-1310 (1994).

[7] E. L. Hamilton, "Attenuation of shear waves in marine sediments," *J. Acoust. Soc. Am.,* **60**, 334-338 (Aug. 1976).

[8] E. L. Hamilton and R. T. Bachman, "Sound velocity and related properties of marine sediments," *J. Acoust. Soc. Am.*, **72**, 1891-1904 (1982).

[9] E. L. Hamilton, "Sound velocity-density relations in sea-floor sediments and rocks," *J. Acoust. Soc. Am.*, **63**, 366-377 (1978).

[10] E. L. Hamilton, "Geoacoustic modelling of the seafloor", *J. Acoust. Soc. Am.*, **68**(5), 1313-1340 (Nov.1980).

[11] A. N. Ivakin, "On sound scattering by multi-scale bottom inhomogeneities", *Oceanology,* **21**(1), 26-27 (1981).

[12] A. N. Ivakin, "Sound scattering by inhomogeneities of an elastic half-space," *Soviet Physics-Acoustics,* **36**(4), 377-380 (1990).

[13] D. R. Jackson and A. N. Ivakin, "Scattering from elastic sea beds: First-order theory," submitted to *J. Acoust. Soc. Am.,* 1996.

[14] D. R. Jackson and K. B. Briggs, "High-frequency bottom backscattering: roughness vs. sediment volume scattering," *J. Acoust. Soc. Am.*, **92**, 962-977 (1992).

[15] E. Y. T. Kuo, "Joint perturbation scattering characterization of a littoral ocean bottom reverberation: Theory, scattering strength predictions, and data comparisons," *IEEE J. Oceanic Engr.,* **20**, 198-210 (July 1995).

[16] A. P. Lyons, A. L. Anderson, and F. S. Dwan, "Acoustic scattering from the seafloor: Modeling and data comparison," *J. Acoust. Soc. Am.,* **95**, 2441-2451 (May 1994).

[17] P. Milholland, M. H. Manghnani, S. O. Schlanger and G. H. Sutton, "Geoacoustic modelling of deep-sea carbonate sediments", *J. Acoust. Soc. Am.*, **68**(5), 1351-1360 (Nov.1980).

[18] P. D. Mourad, and D. R. Jackson, "A model/data comparison for low-frequency bottom backscatter," *J. Acoust. Soc. Am.*, **94**, 344-358 (1993).

[19] M. D. Richardson, E. Muzi, B. Miaschi, and F. Turgutcan, "Shear wave velocity gradients in near-surface marine sediment," in: *Shear Waves in Marine Sediments*, ed. by J. M. Hovem, et al. (Kluwer, Dordrecht, 1991)

[20] M. D. Richardson and K. B. Briggs, "On the use of acoustic impedance values to determine sediment properties," in *Acoustic Classification and Mapping of the Seabed*, ed. by N. G. Pace and D. N. Langhorne, Institute of Acoustics, Bath, 1993, pp.15-25.

[21] T. Yang and S. L. Broschat, "Acoustic scattering from a fluid-elsatic-solid interface using the small slope approximation," *J. Acoust. Soc. Am.*, **96**, 1796-1803 (1994).

[22] T. Yamamoto, "Velocity variabilities and other physical properties of marine sediments measured by crosswell acoustic tomography," *J. Acoust. Soc. Am.*, **98**, 2235-2248 (Oct. 1995).

[23] T. Yamamoto, "Acoustic scattering in the ocean from velocity and density fluctuations in the sediments," *J. Acoust. Soc. Am.*, **99**, 866-879 (Feb. 1996).

[24] A. V. Yefimov, A. N. Ivakin and Yu. P. Lysanov, "A geoacoustic model of sound scattering by the ocean bottom based on deep sea drilling data", *Oceanology*, **28**(3), 290-293 (1988).

Table 1: Parameters defining average, non-fluctuating bulk properties of the illustrative sea bed types.

Descriptive Name	Density Ratio	Compressional Speed Ratio	Shear Speed Ratio	Reference
	m	a_p	a_t	
"Normal" Sand	2.0	1.20 - 0.02i	0.133 - 0.01i	Hamilton (1980)
"Shear" Sand	2.0	1.20 - 0.005i	0.32 - 0.07i	Essen (1994)
Sedimentary Rock	2.5	2.30 - 0.004i	1.30 - 0.11i	Essen (1994)

Table 2: Parameters defining random properties of the illustrative sea bed types.

Sea Bed Type	Volume Spectr. Strength $A^{(v)}$	Volume Spectr. Expon. ξ_v	Volume Aspect Ratio a	Compress. Speed Fluct. Ratio $r_{p\rho}$	Shear Speed Fluct. Ratio $r_{t\rho}$	Rough. Spectr. Strength $A^{(r)}$	Rough. Spectr. Expon. ξ_r
Sand	10^{-5}	1	3	0.1	2.0	10^{-5}	3
Rock	10^{-5}	1	3	3.0	4.0	10^{-5}	3

FIGURES

Figure 1. Geometry relevant to bistatic scattering from a random sea bed.

Figure 2. Backscattering strength as a function of grazing angle for the sedimentary rock example. The fluid case uses identical parameters, except the shear wave speed is set to zero. The abscissa is $\theta_s = \theta_i$ with $\phi_s - \phi_i = 180°$. With the parameters used, there is no frequency dependence. Here and below: (a) roughness scattering, total volume perfectly correlated and total volume uncorrelated scattering, (b) scattering from different types of volume inhomogeneities.

Figure 3. Bistatic scattering strength as a function of scattered grazing angle for the sedimentary rock example. The grazing angle of the incident wave is 45°. The abscissa is θ_s with $\phi_s - \phi_i = 180°$. All parameters are the same as for Fig. 2.

Figure 4. Bistatic scattering strength as a function of scattered azimuth, $\phi_s - \phi_i$, for the sedimentary rock example. The grazing angles of the incident and scattered waves are $\theta_s = \theta_i = 45°$. All parameters are the same as for Fig. 2.

Figure 5. Backcattering strength as a function of grazing angle for the high-shear-speed sand example. The fluid case uses identical parameters, except the shear wave speed is set to zero. The abscissa is $\theta_s = \theta_i$ with $\phi_s - \phi_i = 180°$. With the parameters used, there is no frequency dependence.

Figure 6. Bistatic scattering strength as a function of scattered grazing angle for the high-shear-speed sand example. The abscissa is θ_s with $\phi_s - \phi_i = 180°$. All parameters are the same as for Fig. 5.

Figure 7. Bistatic scattering strength as a function of scattered azimuth, $\phi_s - \phi_i$, for the high-shear-speed sand example. The grazing angles of the incident and scattered waves are $\theta_s = \theta_i = 45°$. All parameters are the same as for Fig. 5.

Figure 8. Backcattering strength as a function of grazing angle for the "normal" sand example. The fluid case uses identical parameters, except the shear wave speed is set to zero. The abscissa is $\theta_s = \theta_i$ with $\phi_s - \phi_i = 180°$. With the parameters used, there is no frequency dependence.

Figure 9. Bistatic scattering strength as a function of scattered grazing angle for the "normal" sand example. Incident grazing angle $\theta_i = 45°$. The abscissa is θ_s with $\phi_s - \phi_i = 180°$. All parameters are the same as for Fig. 8.

Figure 10. Transformation (reflection and transmission) coefficients for

the sedimentary rock example.

Figure 11. Transformation (reflection and transmission) coefficients for the high-speed sand example.

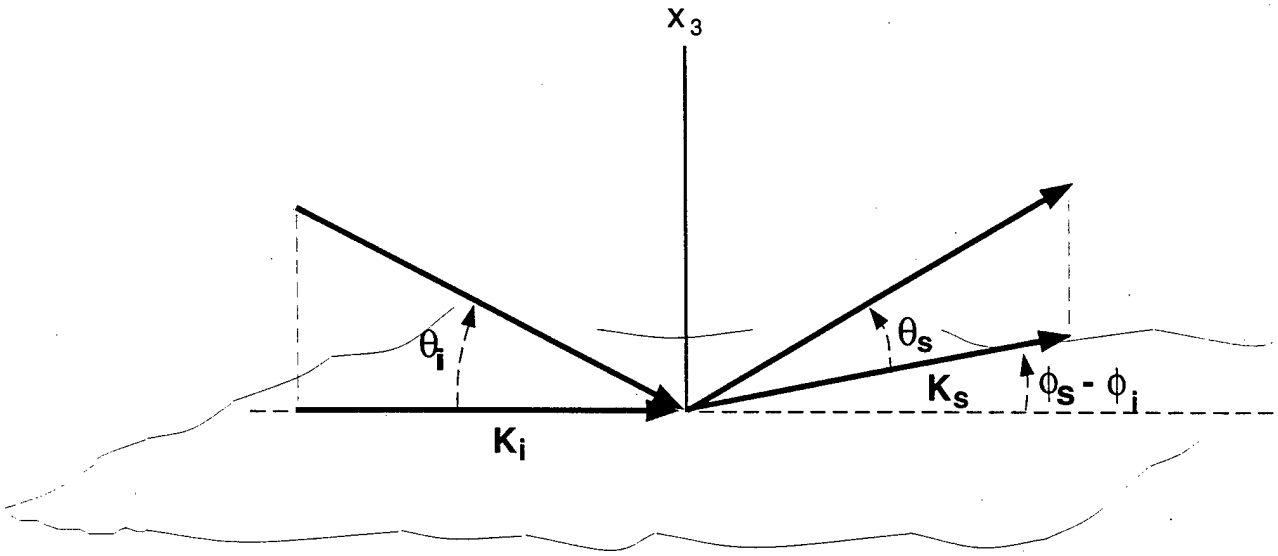

Fig. 1

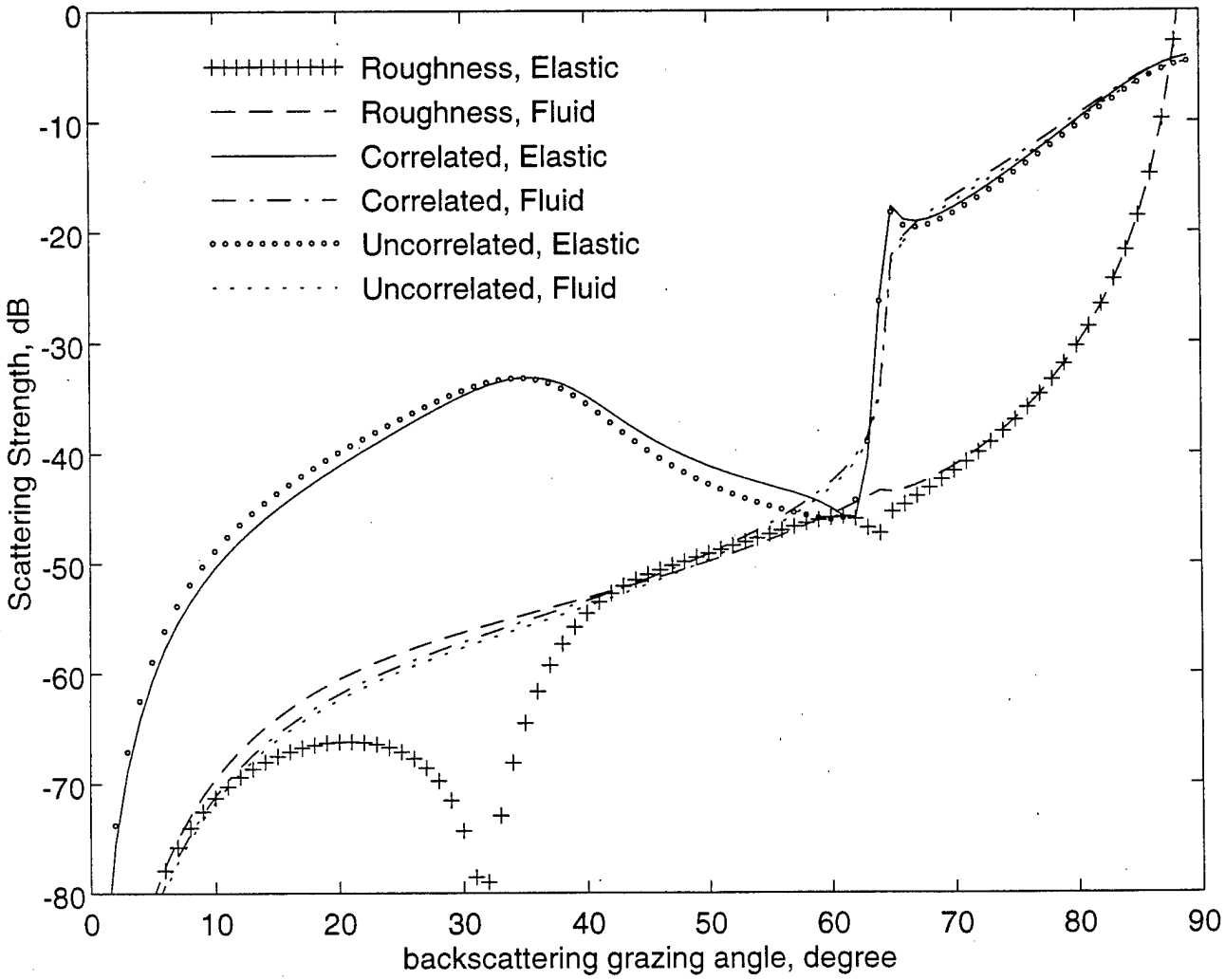
Roughness, Elastic
Roughness, Fluid
Correlated, Elastic
Correlated, Fluid
Uncorrelated, Elastic
Uncorrelated, Fluid
Scattering Strength, dB
backscattering grazing angle, degree
0
-10
-20
-30
-40
-50
-60
-70
-80
0
10
20
30
40
50
60
70
80
90

Fig 2a

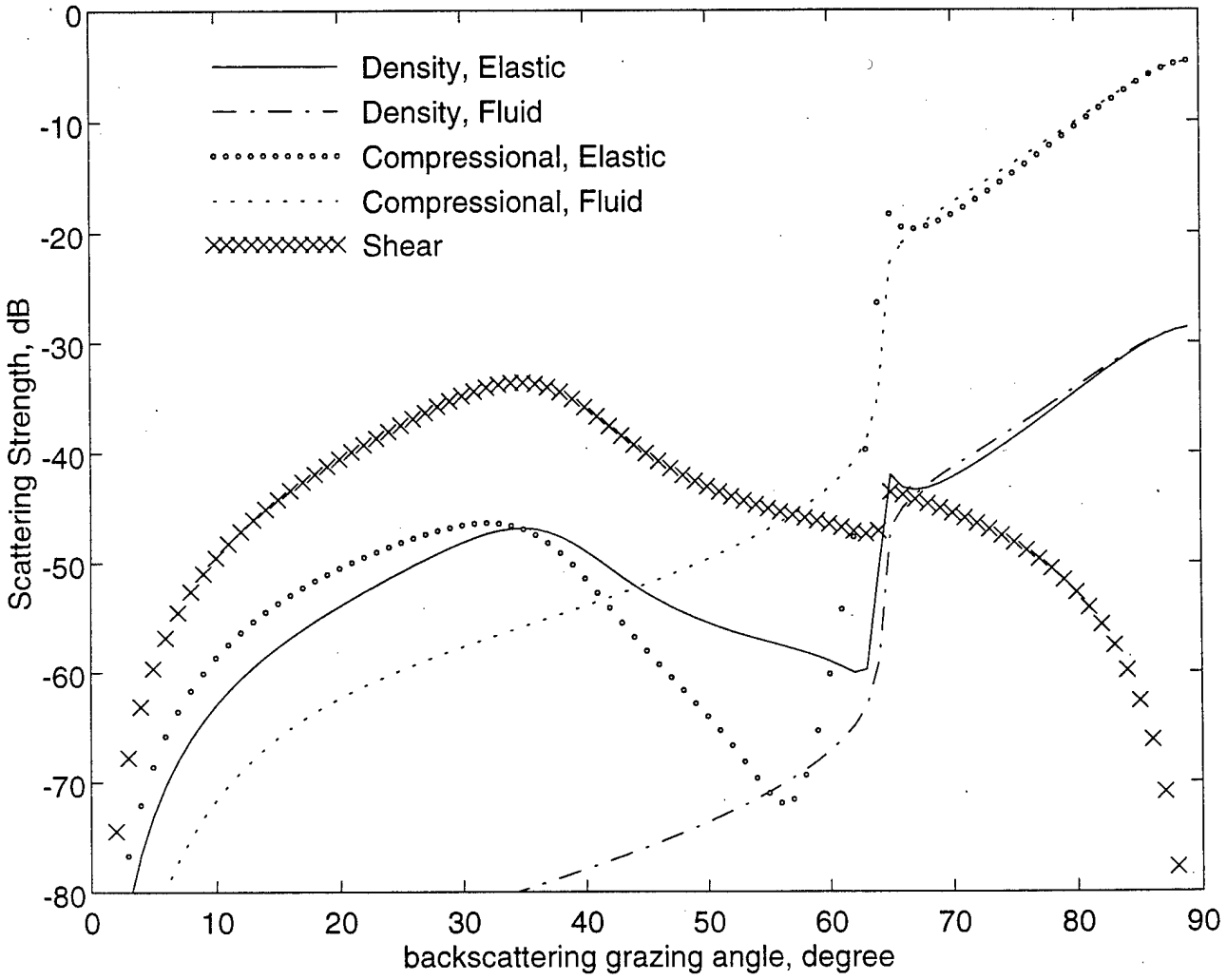
Density, Elastic
Density, Fluid
Compressional, Elastic
Compressional, Fluid
Shear
Scattering Strength, dB
backscattering grazing angle, degree
0
-10
-20
-30
-40
-50
-60
-70
-80
0
10
20
30
40
50
60
70
80
90

Fig. 2b

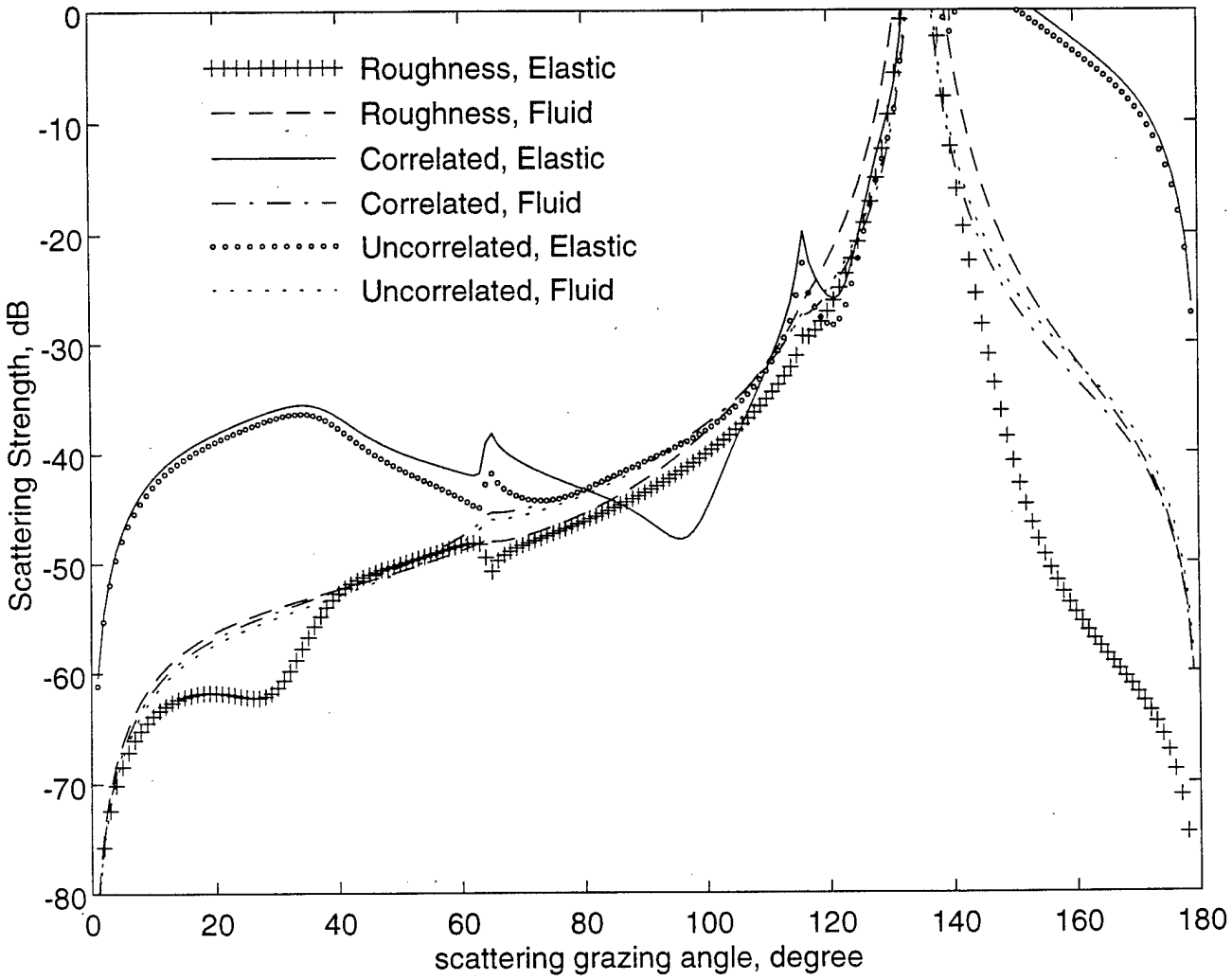
Roughness, Elastic
Roughness, Fluid
Correlated, Elastic
Correlated, Fluid
Uncorrelated, Elastic
Uncorrelated, Fluid
Scattering Strength, dB
0
-10
-20
-30
-40
-50
-60
-70
-80
0
20
40
60
80
100
120
140
160
180
scattering grazing angle, degree

Fig 2a

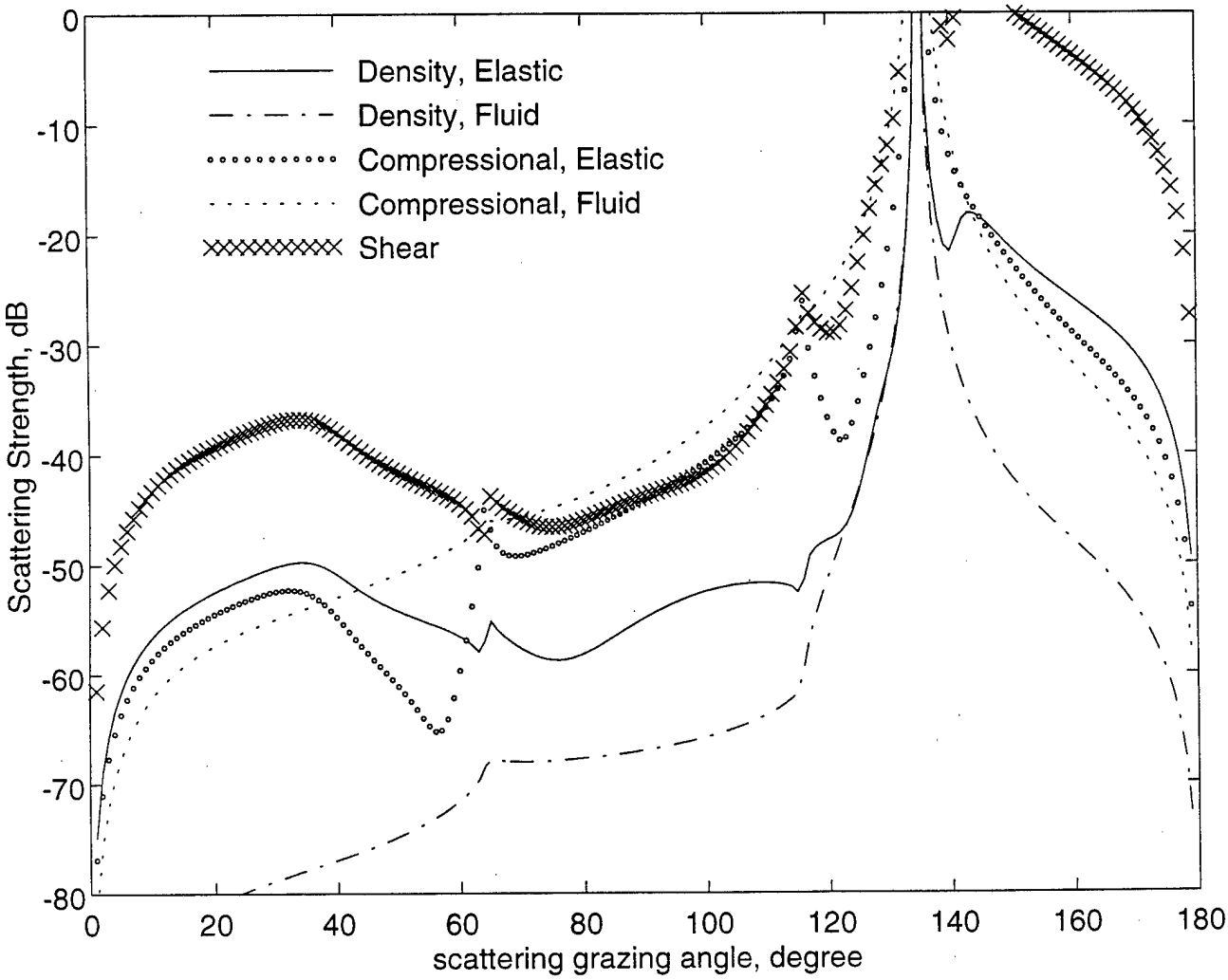
Density, Elastic
Density, Fluid
Compressional, Elastic
Compressional, Fluid
Shear
Scattering Strength, dB
scattering grazing angle, degree
0
-10
-20
-30
-40
-50
-60
-70
-80
0
20
40
60
80
100
120
140
160
180

Fig. 3b

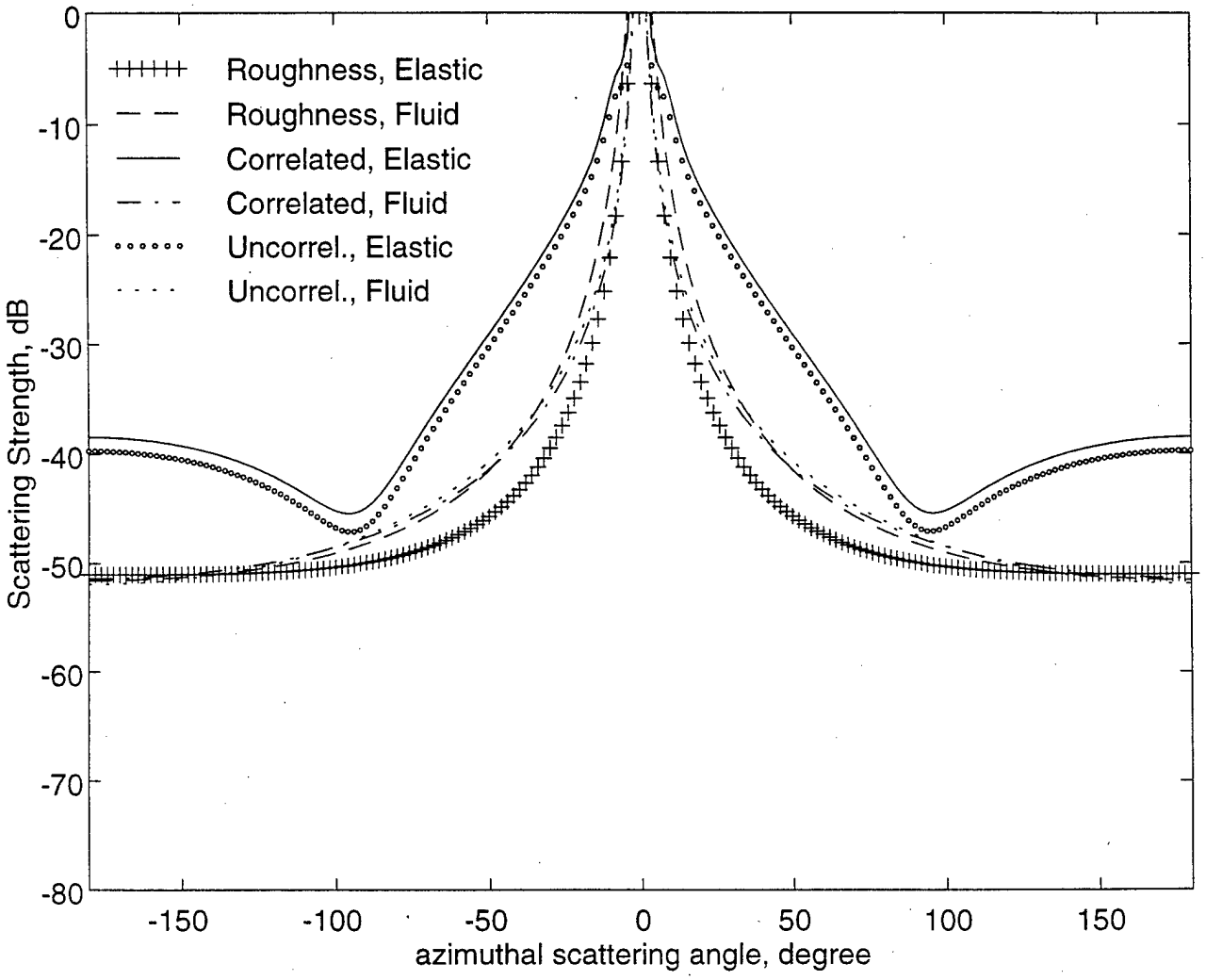
Roughness, Elastic
Roughness, Fluid
Correlated, Elastic
Correlated, Fluid
Uncorrel., Elastic
Uncorrel., Fluid
Scattering Strength, dB
0
-10
-20
-30
-40
-50
-60
-70
-80
-150
-100
-50
0
50
100
150
azimuthal scattering angle, degree

Fig. 4a

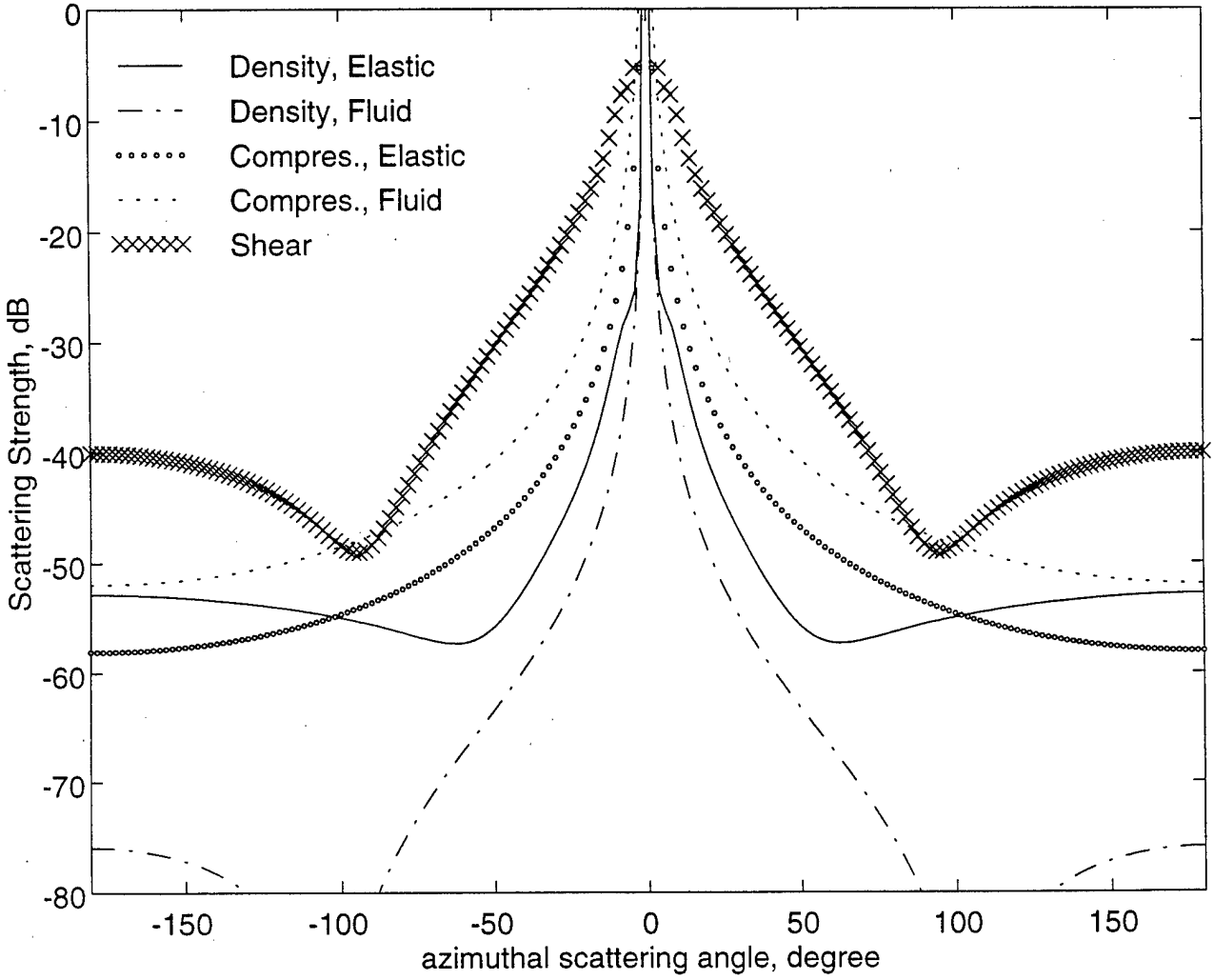
Density, Elastic
Density, Fluid
Compres., Elastic
Compres., Fluid
Shear
Scattering Strength, dB
azimuthal scattering angle, degree
0
-10
-20
-30
-40
-50
-60
-70
-80
-150
-100
-50
0
50
100
150

Fig. 46

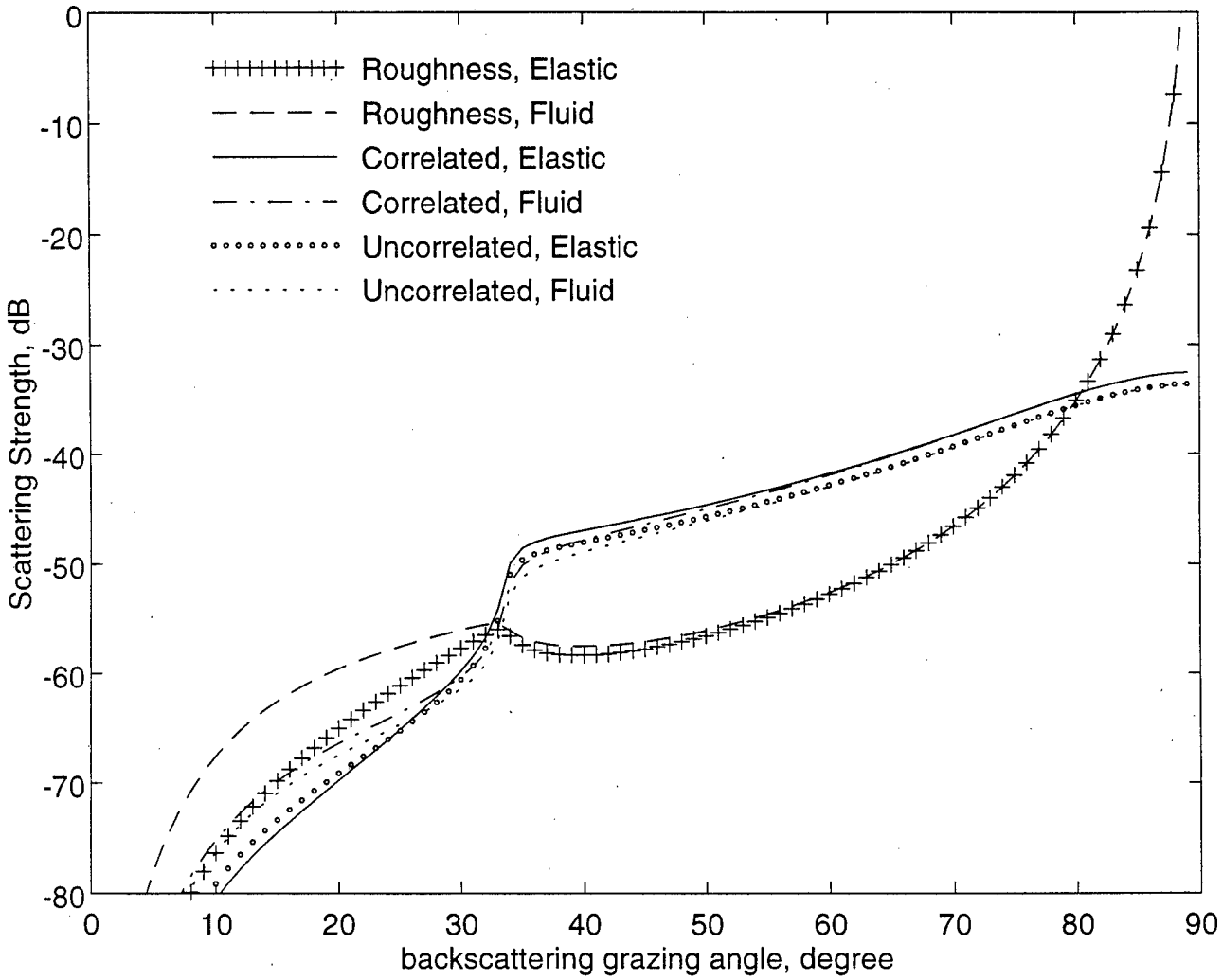
Roughness, Elastic
Roughness, Fluid
Correlated, Elastic
Correlated, Fluid
Uncorrelated, Elastic
Uncorrelated, Fluid
Scattering Strength, dB
0
-10
-20
-30
-40
-50
-60
-70
-80
0
10
20
30
40
50
60
70
80
90
backscattering grazing angle, degree

Fig. 5a

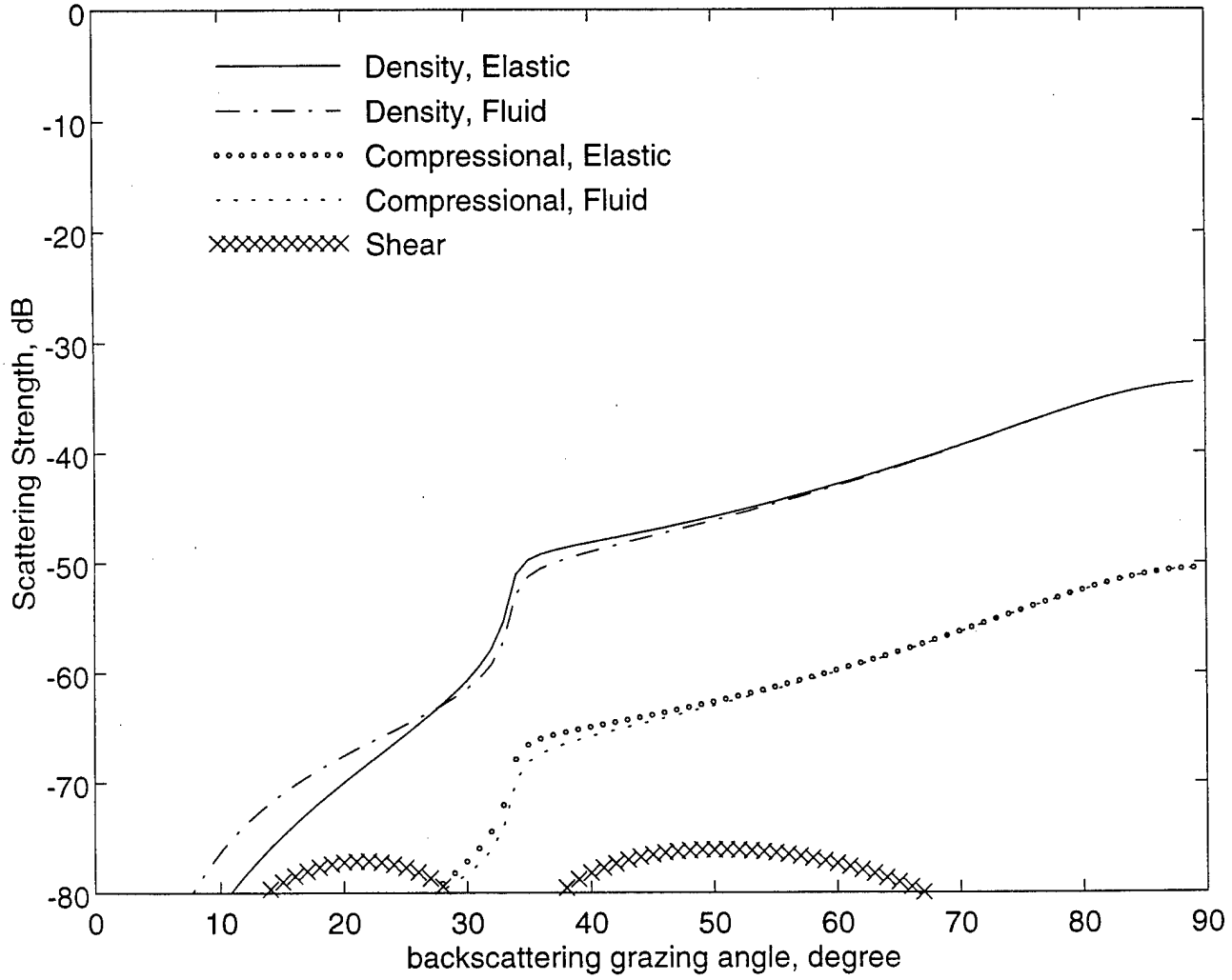
Density, Elastic
Density, Fluid
Compressional, Elastic
Compressional, Fluid
Shear
Scattering Strength, dB
backscattering grazing angle, degree
0
-10
-20
-30
-40
-50
-60
-70
-80
0
10
20
30
40
50
60
70
80
90

Fig. 5b

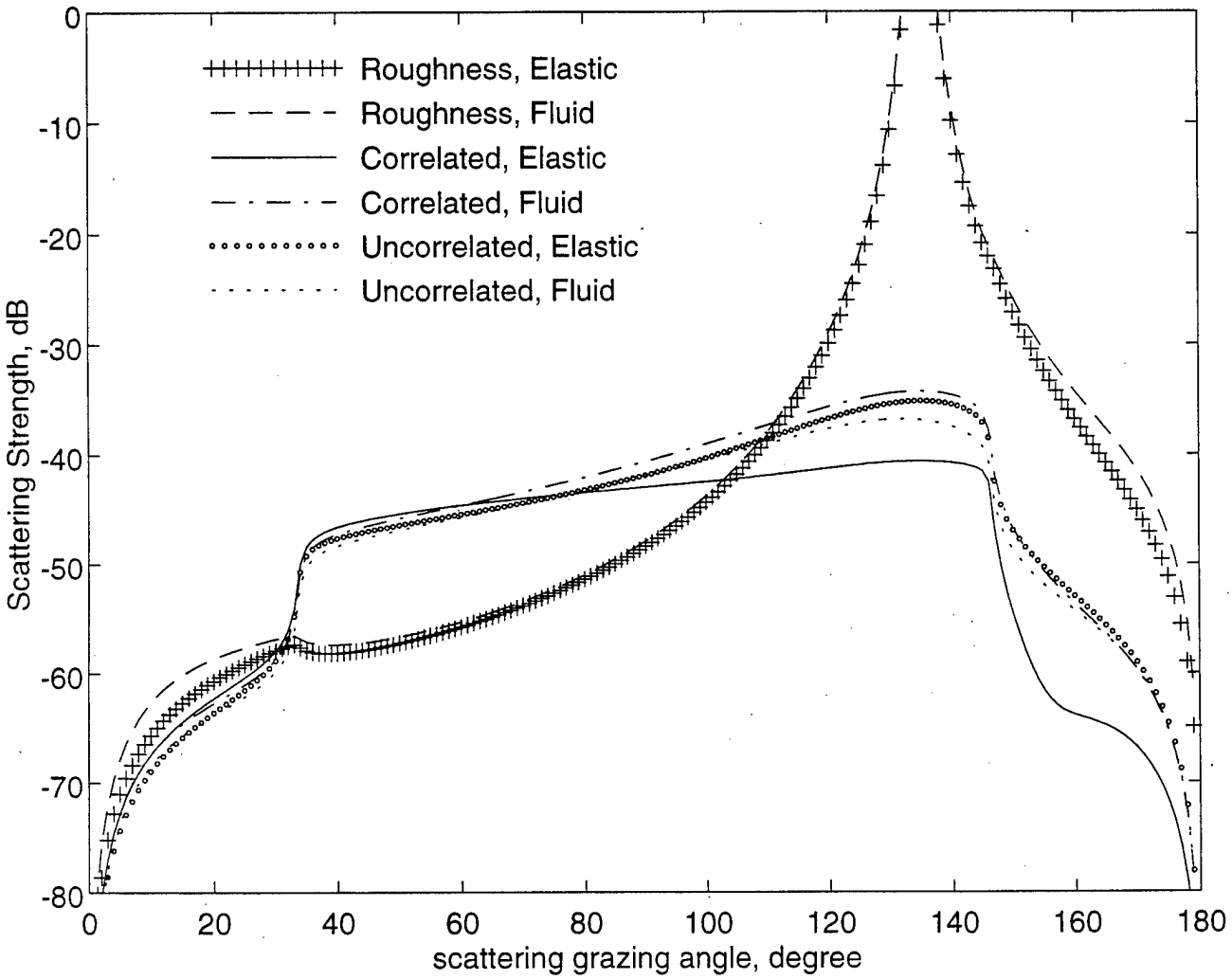
Roughness, Elastic
Roughness, Fluid
Correlated, Elastic
Correlated, Fluid
Uncorrelated, Elastic
Uncorrelated, Fluid
Scattering Strength, dB
0
-10
-20
-30
-40
-50
-60
-70
-80
0
20
40
60
80
100
120
140
160
180
scattering grazing angle, degree

Fig. 6a

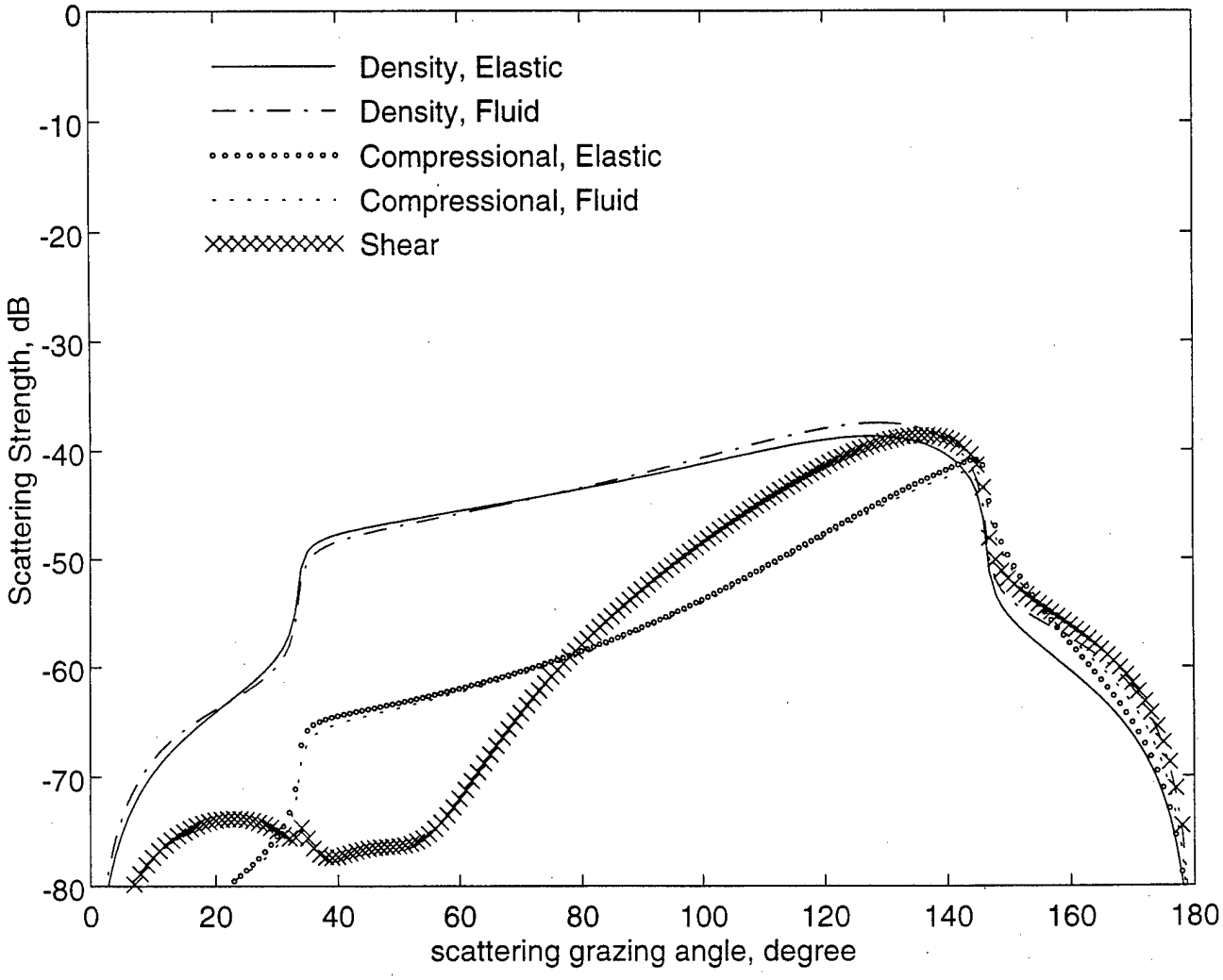
Density, Elastic
Density, Fluid
Compressional, Elastic
Compressional, Fluid
Shear
Scattering Strength, dB
0
-10
-20
-30
-40
-50
-60
-70
-80
0
20
40
60
80
100
120
140
160
180
scattering grazing angle, degree

Fig. 6b

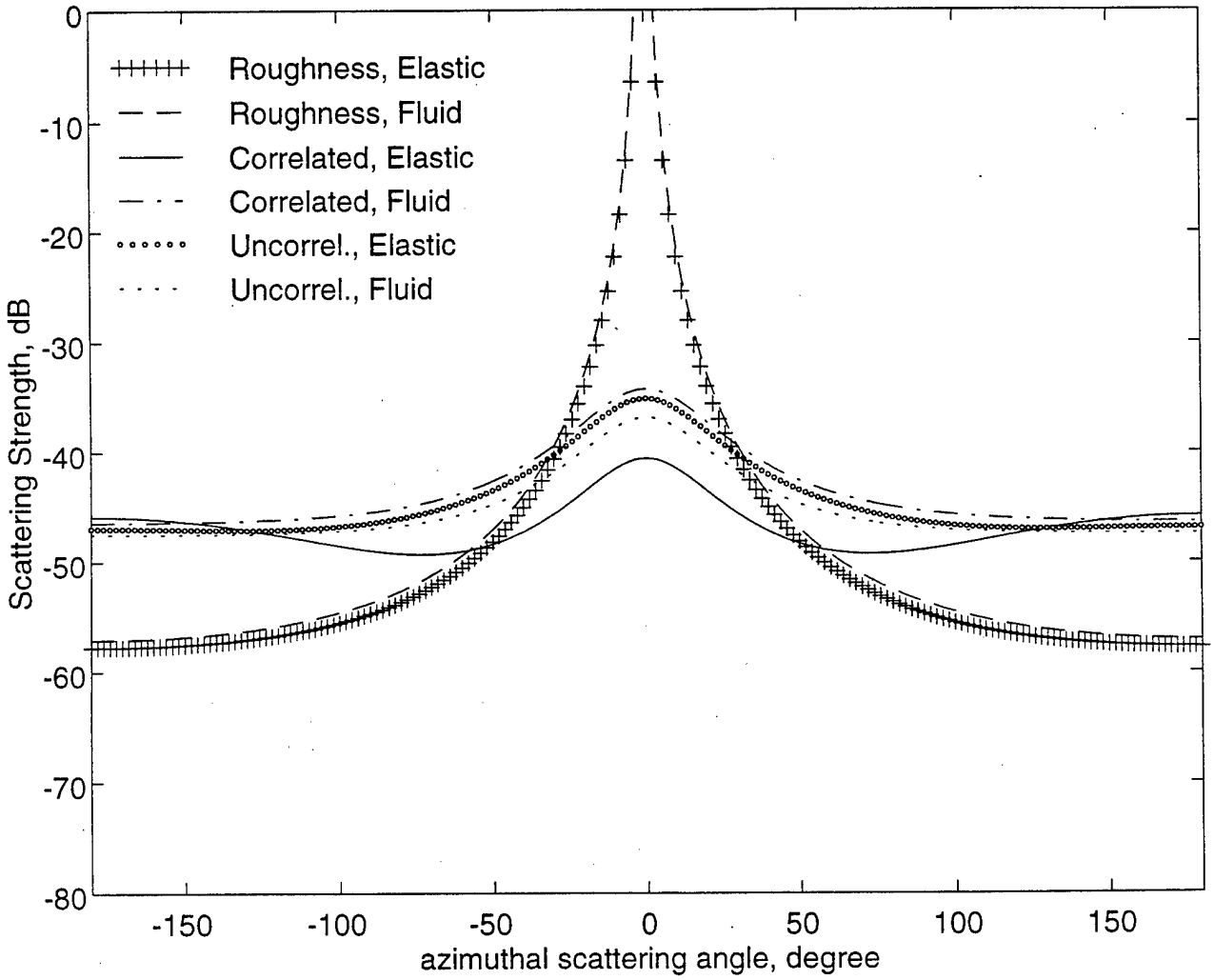
Roughness, Elastic
Roughness, Fluid
Correlated, Elastic
Correlated, Fluid
Uncorrel., Elastic
Uncorrel., Fluid
Scattering Strength, dB
0
-10
-20
-30
-40
-50
-60
-70
-80
-150
-100
-50
0
50
100
150
azimuthal scattering angle, degree

Fig. 2a

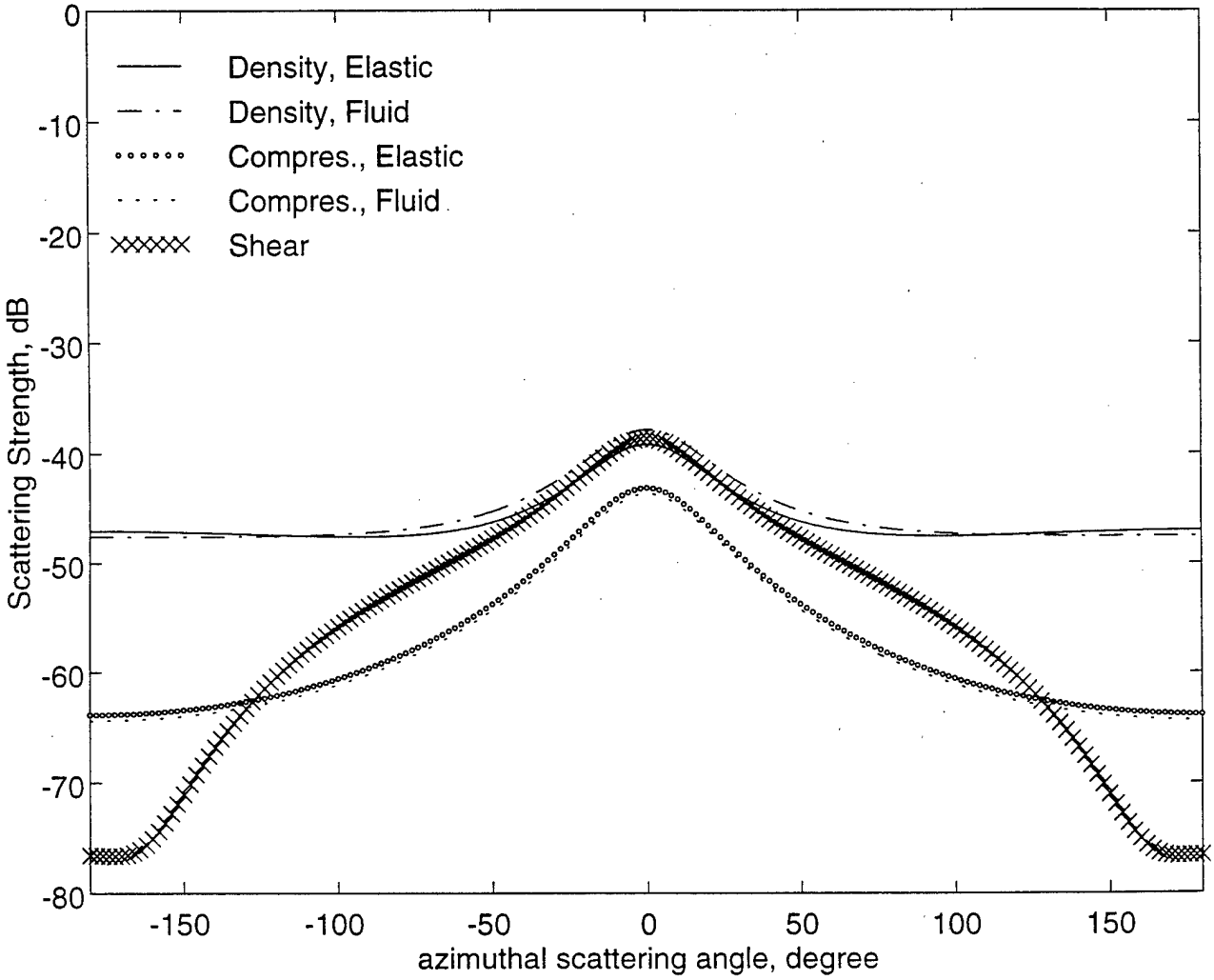
Density, Elastic
Density, Fluid
Compres., Elastic
Compres., Fluid
Shear
Scattering Strength, dB
0
-10
-20
-30
-40
-50
-60
-70
-80
-150
-100
-50
0
50
100
150
azimuthal scattering angle, degree

Fig. 2b

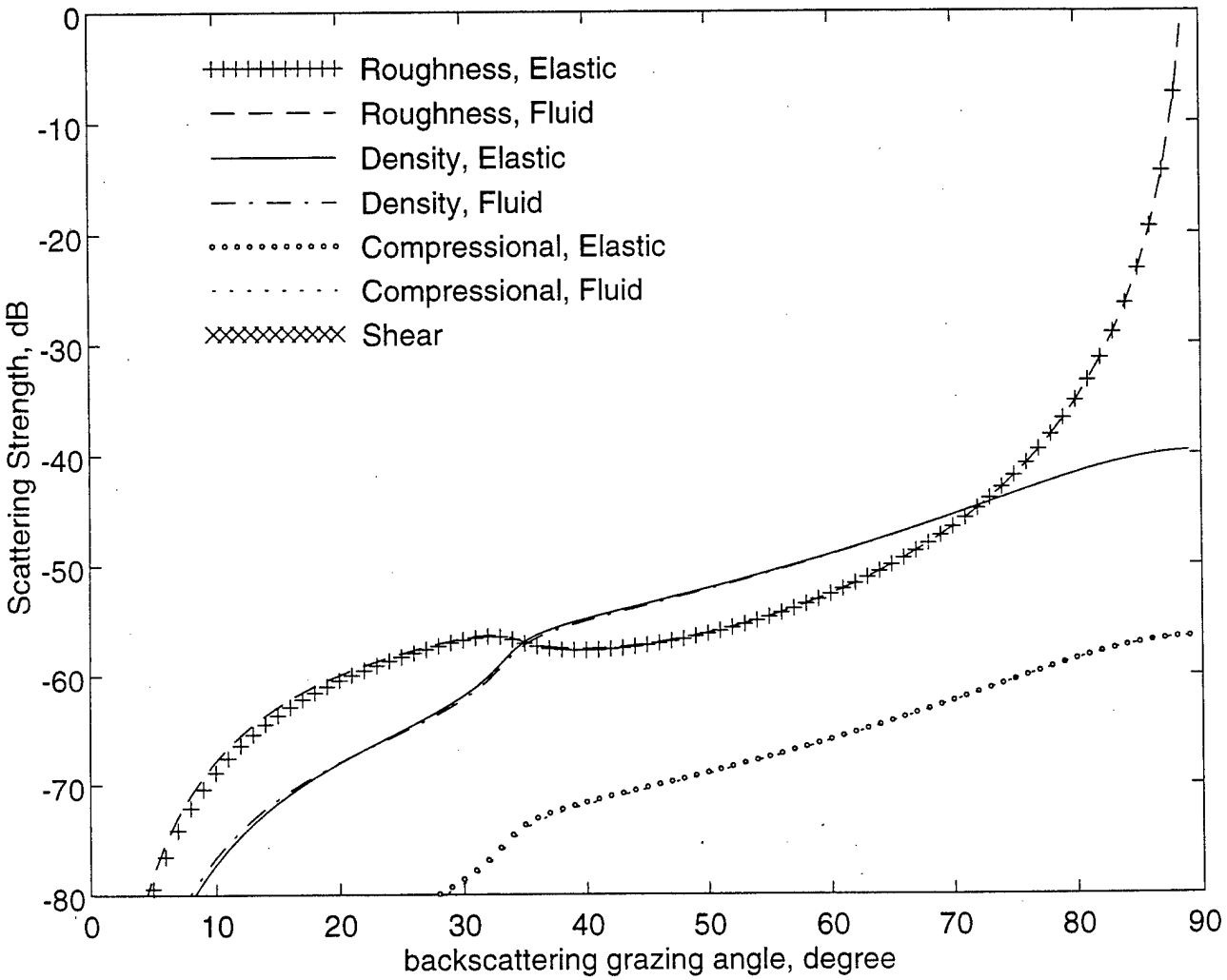
Roughness, Elastic
Roughness, Fluid
Density, Elastic
Density, Fluid
Compressional, Elastic
Compressional, Fluid
Shear
Scattering Strength, dB
0
-10
-20
-30
-40
-50
-60
-70
-80
0
10
20
30
40
50
60
70
80
90
backscattering grazing angle, degree

Fig. 2

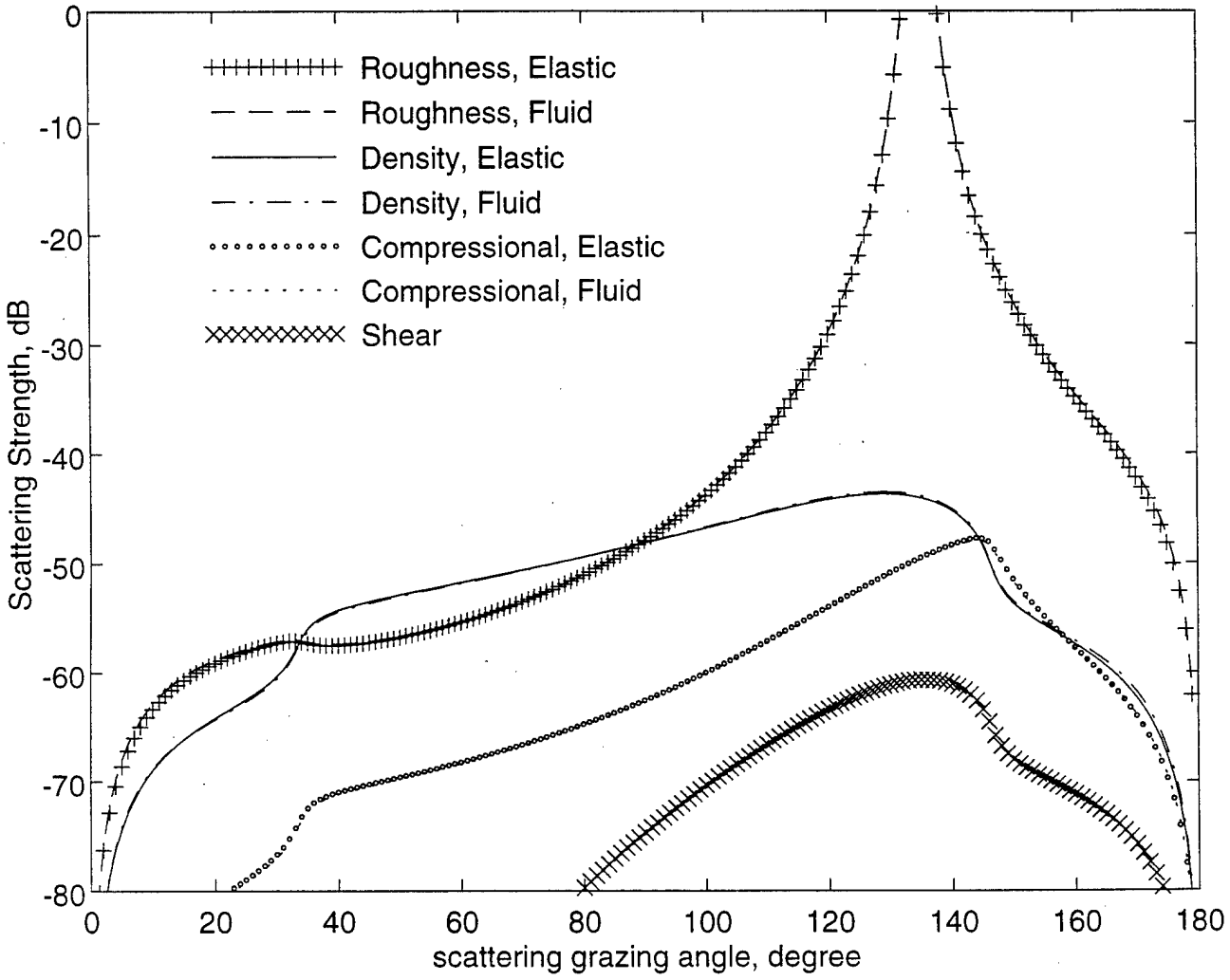
Roughness, Elastic
Roughness, Fluid
Density, Elastic
Density, Fluid
Compressional, Elastic
Compressional, Fluid
Shear
Scattering Strength, dB
0
-10
-20
-30
-40
-50
-60
-70
-80
0
20
40
60
80
100
120
140
160
180
scattering grazing angle, degree

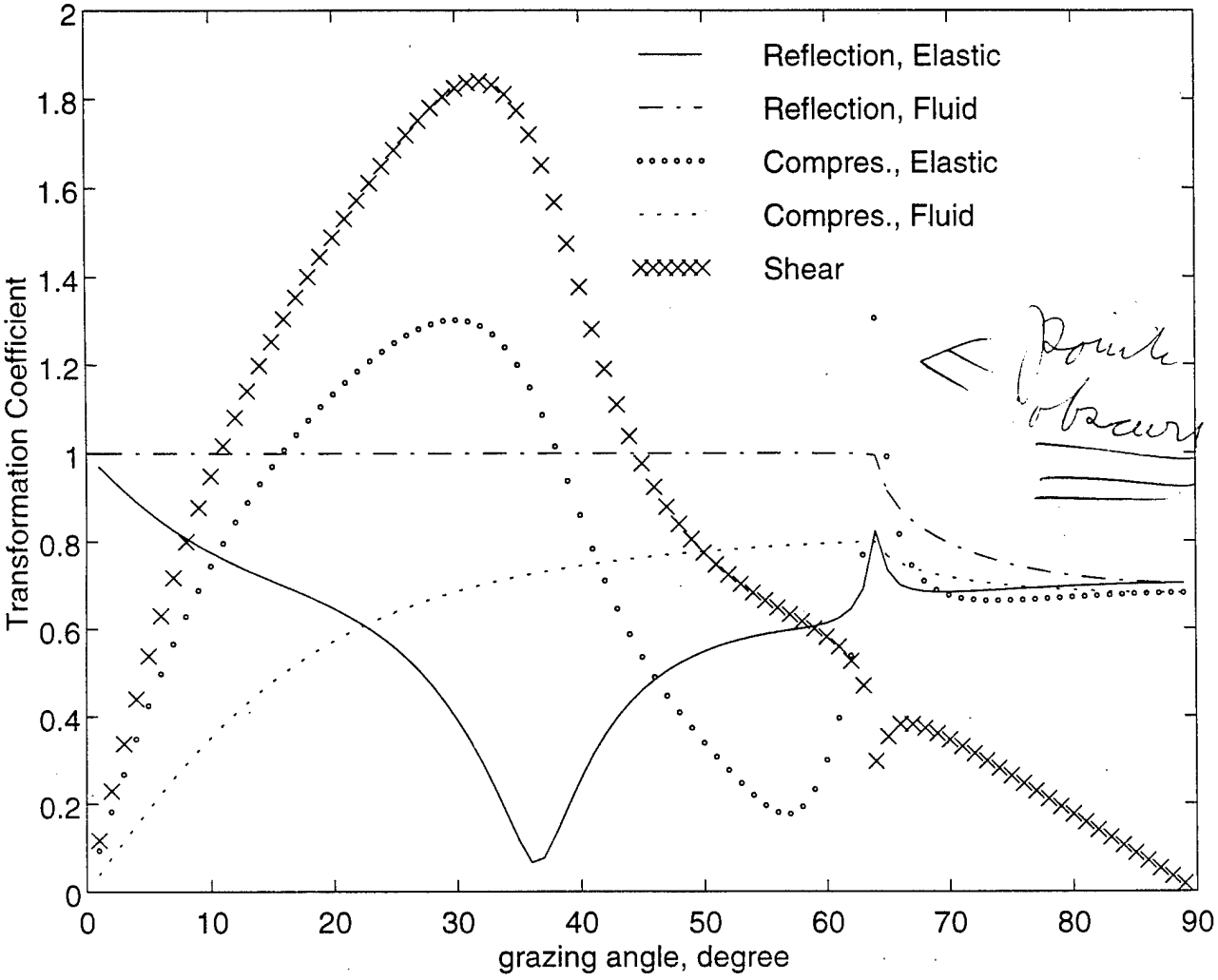
Reflection, Elastic
Reflection, Fluid
Compres., Elastic
Compres., Fluid
Shear
Transformation Coefficient
grazing angle, degree
0
0.2
0.4
0.6
0.8
1
1.2
1.4
1.6
1.8
2
0
10
20
30
40
50
60
70
80
90

Fig. 10

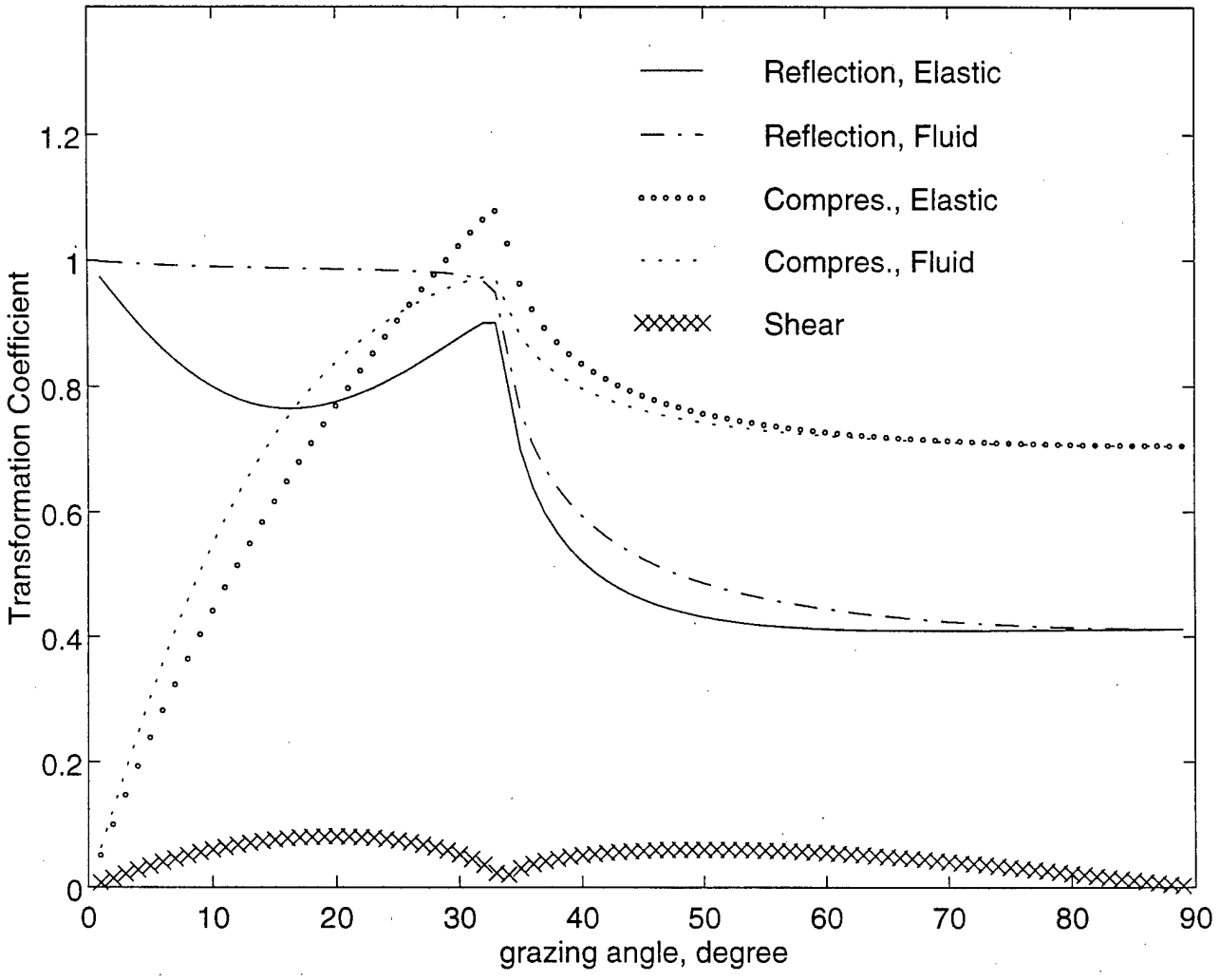
Reflection, Elastic
Reflection, Fluid
Compres., Elastic
Compres., Fluid
Shear
Transformation Coefficient
1.2
1
0.8
0.6
0.4
0.2
0
0
10
20
30
40
50
60
70
80
90
grazing angle, degree

Fig. 11